Scaling patch analysis of planar turbulent mixing layers

Tie Wei, Zhaorui Li and Daniel Livescu

View Online   Export Citation   CrossMark

ARTICLES YOU MAY BE INTERESTED IN

AIP Publishing

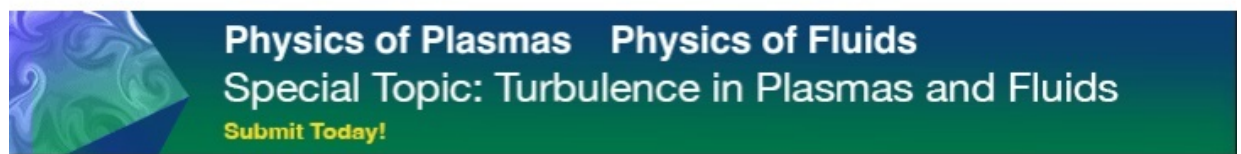# Scaling patch analysis of planar turbulent mixing layers

View Online   Export Citation   CrossMark

Tie Wei,[1,a)] (ID) Zhaorui Li,[2,b)] (ID) and Daniel Livescu[3,c)] (ID)

AFFILIATIONS

[1]Department of Mechanical Engineering, New Mexico Institute of Mining and Technology, 801 Leroy PL, Socorro, New Mexico 87801, USA

[2]Department Of Engineering, Texas A&M University-Corpus Christi, 6300 Ocean Drive, Corpus Christi, Texas 78412, USA

[3]CCS-2, Los Alamos National Laboratory, Los Alamos, New Mexico 87545, USA

[a)]Author to whom correspondence should be addressed: tie.wei@nmt.edu
[b)]Electronic address: zhaorui.li@tamucc.edu
[c)]Electronic address: livescu@lanl.gov

ABSTRACT

Proper scales for the mean flow and Reynolds shear stress in planar turbulent mixing layers are determined from a scaling patch analysis of the mean continuity and momentum equations. By seeking an admissible scaling of the mean continuity equation, a proper scale for the mean transverse flow is determined as $V_{\text{ref}} = (d\delta/dx)U_{\text{ref}}$, where $d\delta/dx$ is the growth rate of the mixing layer width and $U_{\text{ref}} = U_h - U_l$ is the difference between the velocity of the high speed stream U_h and the velocity of the low speed stream U_l. By seeking an admissible scaling for the mean momentum equation, a proper scale for the kinematic Reynolds shear stress is determined as $R_{uv,\text{ref}} = U_{\text{avg}} V_{\text{ref}} = [\frac{1}{2A_u}\frac{d\delta}{dx}]U_{\text{ref}}^2$, where $A_u \overset{\text{def}}{=} (U_h - U_l)/(U_h + U_l)$ is the normalized velocity difference that emerges naturally in the admissible scaling of the mean momentum equation. Self-similar equations for the scaled mean transverse flow V^* and Reynolds shear stress $R_{uv}^* = R_{uv}/R_{uv,\text{ref}}$ are derived from the mean continuity and mean momentum equations. Approximate equations for V^* and R_{uv}^* are developed and found to agree well with experimental data.

Published under an exclusive license by AIP Publishing. https://doi.org/10.1063/5.0122494

I. INTRODUCTION

A two-dimensional (2D) planar turbulent mixing layer occurs when two parallel streams at different speeds move upon each other, as illustrated in Fig. 1. Instabilities develop along the interface and the ensuing eddy motions drive the growth of a mixing layer. Mixing layers play a vital role in combustion engines including, for example, in air-breathing hypersonic vehicles. The size and weight of the supersonic combustion scramjet are constrained in part by how rapidly the fuel and oxidizer can be mixed to enable complete combustion. On the theoretical and modeling side, as one of the most fundamental free-shear flows, the planar mixing layer has been used, among other things, as a benchmark for evaluating turbulence models.[1,2]

The first analytical study of a mixing layer was carried out by Görtler in 1942.[4] Applying Prandtl's eddy viscosity model, Görtler derived an analytic solution for the planar turbulent mixing layer. The details of Görtler's analysis can be found in Ref. 5. Townsend[1] showed that the governing equations and boundary conditions for the planar

turbulent mixing layer can yield "self-similar" solutions for the flow in the far field at sufficiently high Reynolds number. Over the past seven decades, numerous researchers have studied this canonical flow theoretically, experimentally, and numerically.[1,6–31] A comprehensive summary of mixing layer research is provided by Pope.[2] Despite intensive research, however, our understanding of this apparently simple flow is still incomplete.

A long-standing question in studies of turbulent mixing layers, as stated by Champagne *et al.*[10] in 1976, is "... *whether there exist in the two-dimensional mixing layer universal self-preserving distributions of the mean velocity, turbulence intensities and other mean quantities not determined by viscous effects.*" Spencer[32] and Yule[33] reported experimentally determined contradictory trends in the variation of the asymptotic peak Reynolds stress values. Two conjectures have been put forward to explain the lack of a "universal" self-similar state at a high Reynolds number:[14,16,34] (1) effects of the initial condition, e.g., the presence or lack of a trip wire, state and thickness of the initial
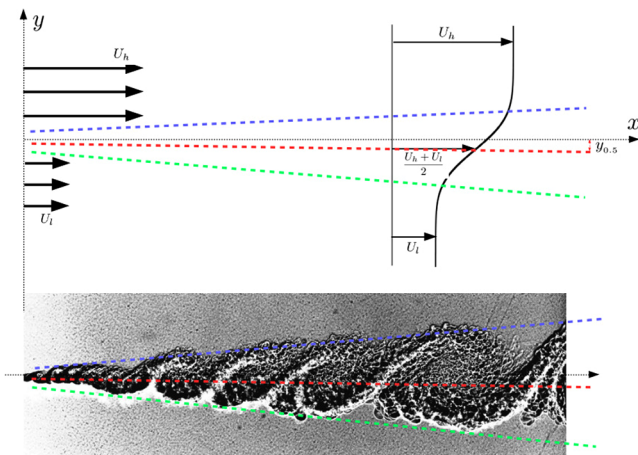
FIG. 1. Schematic of a planar mixing layer. The photograph (bottom) is by Rebello (see Ref. 3, p. 177). U_h is the velocity of the high speed stream, U_l is the velocity of the low speed stream, and the average speed is $U_{avg} = 0.5(U_h + U_l)$. $y_{0.5}$ is the distance from the x axis to the location where the mean axial velocity is U_{avg}. See also Fig. 5.23 in Ref. 2 for the curves of the upper edge, lower edge, and $y_{0.5}$ locations.

boundary layer, and the free-stream turbulence intensity and (2) effects of boundary conditions, such as the end-plate or top/bottom walls in the wind tunnel.[14]

In this work, proper scales for the mean flow and Reynolds shear stress in planar turbulent mixing layers are determined using a scaling patch approach. Under proper scaling, we demonstrate that the mean flow and Reynolds shear stress approach a self-similar state in the far fields of planar turbulent mixing layers, but the self-similar functions depend on the difference in the velocities of the two streams. In Sec. II, the governing equations are first presented, and the scaling patch approach is then applied. Approximate equations for the scaled mean transverse flow and Reynolds shear stress are derived. In Sec. III, the approximated equations are validated against experimental data. Section IV summarizes the work.

II. SCALING PATCH ANALYSIS OF PLANAR TURBULENT MIXING LAYERS

In this work, we consider the simplest mixing layer flow: a two-dimensional planar mixing layer developing from two fluids of the same density and viscosity. The velocity of the high speed stream is denoted as U_h and the velocity of the low speed stream as U_l. Conventionally, the difference between the two velocities is characterized by the velocity ratio (see, e.g., Mehta[16]),

$$ r \overset{\text{def}}{=} \frac{U_l}{U_h}. \tag{1} $$

Here, we introduce another dimensionless number to characterize the velocity difference in a mixing layer as

$$ A_u \overset{\text{def}}{=} \frac{U_h - U_l}{U_h + U_l} = \frac{1 - r}{1 + r}. \tag{2} $$

A_u is bounded between 0 (two streams with $U_h = U_l$) and 1 (one of the stream is still or $U_l = 0$). This definition of the normalized velocity

difference A_u is analogous to the definition of the Atwood number for the Rayleigh–Taylor instability.[35–37] A_u has been used in previous studies of mixing layers, often using the symbol λ, e.g., in Abramovich et al.,[38] Sabin,[39] and Birch and Eggers,[8] but the significance of A_u has not previously been fully recognized. In the following analysis, we demonstrate that A_u plays an important role in the understanding and scaling of turbulent mixing layers.

Turbulent mixing layers are slender, that is, they spread slowly in the transverse direction,[2,5] and can therefore be studied using Prandtl's boundary layer equations. Here, we consider incompressible and single phase flow, and the mean continuity equation and mean momentum equation in the streamwise direction are[1,2,5,38]

$$ 0 = \frac{\partial U}{\partial x} + \frac{\partial V}{\partial y}, \tag{3a} $$

$$ 0 = -U\frac{\partial U}{\partial x} - V\frac{\partial U}{\partial y} + \frac{\partial R_{uv}}{\partial y} + \frac{\partial(R_{uu} - R_{vv})}{\partial x} + \nu\frac{\partial^2 U}{\partial y^2} - \frac{1}{\rho}\frac{\partial P}{\partial x}. \tag{3b} $$

As illustrated in Fig. 1, x and y are the axial and transverse coordinates, respectively. The upper case letter U is the mean velocity in the streamwise direction, and V is the mean transverse velocity. The kinematic Reynolds shear stress is denoted as $R_{uv} = -\langle uv \rangle$, where the angle brackets $\langle \rangle$ denote Reynolds averaging, and the lower case letters u and v are the velocity fluctuations in the streamwise and transverse directions, respectively. $R_{uu} = -\langle uu \rangle$ and $R_{vv} = -\langle vv \rangle$ are the Reynolds normal stresses in the x- and y-directions, respectively. ν is the fluid kinematic viscosity. For turbulent mixing layer at high Reynolds numbers, it can be shown that the viscous force and turbulent force term $\partial(R_{uu} - R_{vv})/\partial x$ are negligible in the far field.[1] In this work, we assume that there is no mean pressure gradient imposed on the flow field. The boundary conditions for the planar turbulent mixing layers are listed in Table I.

A prominent feature of the planar mixing layer, unlike the planar jets or wakes, is that it does not develop evenly on the two sides. A mixing layer spreads preferentially toward the low speed side, as illustrated in Fig. 1. The location where the mean streamwise velocity equals the average velocity is denoted as $y_{0.5}$: $U(y = y_{0.5}) = U_{avg}$. Figure 1 shows that, as the mixing layer develops downstream, $y_{0.5}$ shifts away from the horizontal axis toward the low speed side. To transform the flow to a self-similar state, the coordinate system has to be shifted. The origin in the transformed coordinate system is at $O' = (x_{0.5}, y_{0.5})$, as sketched in Fig. 2, where $x_{0.5}$ is moving downstream at the speed of U_{avg}. For a planar mixing layer to reach a self-similar state, the mean transverse velocity of O', i.e., $V_{o'}$ has to be constant. That is, the shift angle in Fig. 2 is constant as supported by the experimental measurements of Champagne et al.[10] (see Fig. 5.23 in Ref. 40).

The transformed coordinates and velocity components are denoted as

TABLE I. Boundary conditions for turbulent mixing layer.

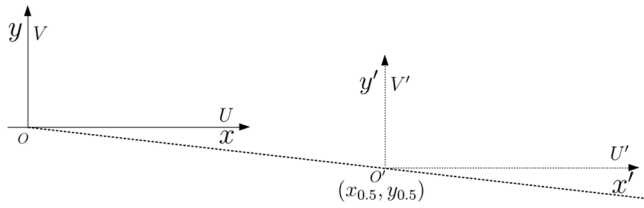|			
$y = +\infty$	$U = U_h$;	$V = V_{+\infty}$;	$R_{uv} = 0$.
$y = -\infty$	$U = U_l$;	$V = V_{-\infty}$;	$R_{uv} = 0$.

FIG. 2. Transformation of coordinate systems for a planar mixing layer.

$$x' = x - x_{0.5}, \quad y' = y - y_{0.5}, \tag{4}$$

$$U' = U - U_{o'} = U - U_{avg}, \quad V' = V - V_{o'}. \tag{5}$$

The self-similar variables used here are defined as

$$\xi \overset{\text{def}}{=} \frac{y'}{\delta} = \frac{y - y_{0.5}(x)}{\delta(x)}, \tag{6}$$

$$U^*(\xi) \overset{\text{def}}{=} \frac{U'}{U_{ref}} = \frac{U(x,y) - U_{avg}}{U_{ref}(x)}, \tag{7}$$

$$V^*(\xi) \overset{\text{def}}{=} \frac{V'}{V_{ref}} = \frac{V(x,y) - V_{o'}}{V_{ref}(x)}, \tag{8}$$

$$R_{uv}^*(\xi) \overset{\text{def}}{=} \frac{R_{uv}(x,y)}{R_{uv,ref}(x)}, \tag{9}$$

where δ is the width of the mixing layer and $U_{ref}, V_{ref}, R_{uv,ref}$ are the reference scale for the mean axial flow, mean transverse flow, and Reynolds shear stress, respectively.

The references scales U_{ref}, V_{ref}, and $R_{uv,ref}$ will be obtained by a scaling patch approach, a relatively new method developed by Fife *et al.* for shear-driven wall-bounded turbulence.[41–43] The scaling patch approach has been applied to obtain proper scaling in the passive scalar transport in turbulent pipe or channel flow,[44,45] turbulent boundary flow with roughness,[46] turbulent Taylor–Couette flow,[47] buoyancy-driven turbulence convection,[48,49] and recently to free shear turbulence including jets,[50] plumes,[51] and wakes.[52] Here, an admissible scaling is sought for the mean continuity and momentum equations, as well as the normalized boundary conditions.

To transform the governing equations into the similarity variables, we first note that the derivatives of ξ with respect to x and y are

$$\frac{\partial \xi}{\partial x} = -\frac{1}{\delta}\frac{dy_{0.5}}{dx} - \frac{1}{\delta}\frac{d\delta}{dx}\xi, \tag{10a}$$

$$\frac{\partial \xi}{\partial y} = \frac{1}{\delta}. \tag{10b}$$

Then, the derivative of U with respect to x is

$$\frac{\partial U}{\partial x} = -\frac{U_{ref}}{\delta}\frac{dy_{0.5}}{dx}\frac{dU^*}{d\xi} - \frac{U_{ref}}{\delta}\frac{d\delta}{dx}\xi\frac{dU^*}{d\xi} + \frac{dU_{ref}}{dx}U^*, \tag{11}$$

and the derivatives of U, V, and R_{uv} with respect to y are

$$\frac{\partial U}{\partial y} = \frac{U_{ref}}{\delta}\frac{dU^*}{d\xi}, \tag{12a}$$

$$\frac{\partial V}{\partial y} = \frac{V_{ref}}{\delta}\frac{dV^*}{d\xi}, \tag{12b}$$

$$\frac{\partial R_{uv}}{\partial y} = \frac{R_{uv,ref}}{\delta}\frac{dR_{uv}^*}{d\xi}. \tag{12c}$$

Using the self-similar variables, the dimensionless boundary conditions for the mixing layer are listed in Table II. A natural choice for U_{ref} is then $U_{ref} = U_h - U_l$, because the boundary conditions for U^* become $U^*|_{\xi=\infty} = 0.5$ and $U^*|_{\xi=-\infty} = -0.5$; both are of $O(1)$. In a planar turbulent mixing layer without external pressure gradient, $U_h - U_l$ is a constant and $dU_{ref}/dx = 0$. Therefore, the last term in Eq. (11) is zero.

Substituting the self-similar variables and their derivatives into Eqs. (3a) and (3b), the mean continuity equation and the mean momentum equation can be presented as

$$0 = -\frac{U_{ref}}{\delta}\frac{dy_{0.5}}{dx}\frac{dU^*}{d\xi} - \frac{U_{ref}}{\delta}\frac{d\delta}{dx}\xi\frac{dU^*}{d\xi} + \frac{V_{ref}}{\delta}\frac{dV^*}{d\xi}, \tag{13a}$$

$$0 = (U_{avg} + U_{ref}U^*)\left(\frac{V_{ref}}{\delta}\frac{dV^*}{d\xi}\right) - (V_{o'} + V_{ref}V^*)\left(\frac{U_{ref}}{\delta}\frac{dU^*}{d\xi}\right)$$
$$+ \left(\frac{R_{uv,ref}}{\delta}\right)\frac{dR_{uv}^*}{d\xi}. \tag{13b}$$

Note that in the derivation of Eq. (13b), the term $\partial U/\partial x$ in the mean momentum Eq. (3b) is substituted by $-\partial V/\partial y$ via the continuity equation. Next, we will seek an admissible scaling of the mean continuity equation, and then an admissible scaling of the mean momentum equation.

A. Admissible scaling of the mean continuity equation

Multiplying δ/V_{ref} onto the mean continuity Eq. (13a) yields a dimensionless equation as

$$0 = -\left[\frac{U_{ref}}{V_{ref}}\frac{dy_{0.5}}{dx}\right]\frac{dU^*}{d\xi} - \left[\frac{U_{ref}}{V_{ref}}\frac{d\delta}{dx}\right]\xi\frac{dU^*}{d\xi} + \frac{dV^*}{d\xi}. \tag{14}$$

The nominal orders of magnitude of the three terms on the right side of Eq. (14) are $U_{ref}/V_{ref}\, dy_{0.5}/dx$, $U_{ref}/V_{ref}\, d\delta/dx$, and 1. For Eq. (14) to satisfy the requirement of an admissible scaling, i.e., at least two terms with a nominal order of magnitude 1, a scale for the mean transverse flow is $(d\delta/dx)U_{ref}$ or $(dy_{0.5}/dx)U_{ref}$. Here, we set the reference scale for the mean transverse velocity as

$$V_{ref} \overset{\text{def}}{=} U_{ref}\frac{d\delta}{dx} = (U_h - U_l)\frac{d\delta}{dx}, \tag{15}$$

and denote the ratio of the pre-factors to the first two terms in Eq. (14) as

$$B \overset{\text{def}}{=} \frac{\dfrac{dy_{0.5}}{dx}}{\dfrac{d\delta}{dx}}. \tag{16}$$

TABLE II. Boundary conditions for the dimensionless equations for planar turbulent mixing layers.

$\xi = -\infty$	$U^* = \dfrac{-0.5(U_h - U_l)}{U_{ref}}$,	$V^* = \dfrac{V_{-\infty} - V_{o'}}{V_{ref}}$,	$R_{uv}^* = 0.$
$\xi = \infty$	$U^* = \dfrac{0.5(U_h - U_l)}{U_{ref}}$,	$V^* = \dfrac{V_{\infty} - V_{o'}}{V_{ref}}$,	$R_{uv}^* = 0.$

Hence, an admissible scaling of the mean continuity equation is

$$0 = -B\frac{dU^*}{d\xi} - \xi\frac{dU^*}{d\xi} + \frac{dV^*}{d\xi}. \tag{17}$$

Equation (17) shows that, for V^* to be self-similar, it is necessary that B is a constant (does not vary with x). In the present coordinate system, the positive y direction is from the low-speed side to the high-speed side. Thus, B is negative because $dy_{0.5}/dx$ is negative. Experimental data indicate (see Sec. III) that B is indeed a constant, but its value varies in the range of $-0.25 \lesssim B \leq 0$ depending on A_u.

Integrating the mean continuity Eq. (17) and applying boundary conditions produces an analytic equation for the scaled mean transverse velocity V^* as

$$V^* = B(U^* + 0.5) + \int_{-\infty}^{\xi}\left(\xi\frac{dU^*}{d\xi}\right)d\xi + V^*_{-\infty}. \tag{18}$$

If U^* exhibits a self-similar state (a function of ξ only), Eq. (18) indicates that V^* will be a function of ξ and B only. In other words, the scaled mean transverse velocity V^* will also approach a self-similar state, but V^* varies with A_u and is not universal.

Integrating the mean continuity Eq. (17) from $\xi = -\infty$ to $\xi = +\infty$ yields a relation between the mean transverse velocity at the upper and lower edges of the mixing layer as

$$V^*_\infty - V^*_{-\infty} = B + \int_{-\infty}^{\infty}\left(\xi\frac{dU^*}{d\xi}\right)d\xi. \tag{19}$$

Empirically, it is observed that U^* is approximately anti-symmetric (see Fig. 5). Therefore, the second term on the right of Eq. (19) is close to 0 and $V^*_\infty - V^*_{-\infty} \approx B$.

B. Admissible scaling of the mean axial-momentum equation

Multiplying $\delta/(U_{avg}V_{ref})$ onto the mean momentum Eq. (13b) yields a dimensionless equation as

$$0 = \frac{dV^*}{d\xi} - \left[2A_u\frac{V_{o'}}{V_{ref}}\right]\frac{dU^*}{d\xi} + [2A_u]\left(U^*\frac{dV^*}{d\xi} - V^*\frac{dU^*}{d\xi}\right)$$
$$+ \left[\frac{R_{uv,ref}}{U_{avg}V_{ref}}\right]\frac{dR^*_{uv}}{d\xi}. \tag{20}$$

Equation (20) represents the balance of two forces: the advective or inertial force (the first three terms on the right side) and the turbulent force (last term). For Eq. (20) to be an admissible scaling, the pre-factor to the turbulence term must have a nominal order of magnitude 1. Hence, a proper scale for the Reynolds shear stress is

$$R_{uv,ref} \stackrel{\text{def}}{=} U_{avg}V_{ref} = \frac{U_{avg}}{U_{ref}}U_{ref}V_{ref} = \left[\frac{1}{2A_u}\frac{d\delta}{dx}\right]U^2_{ref}. \tag{21}$$

Note that in many previous studies of turbulent mixing layers, R_{uv} is normalized by U^2_{ref}, but Pantano and Sakar[40] and Baltzer and Livescu[53] have pointed out the importance of $d\delta/dx$ in the proper scaling of R_{uv}.

Substituting the definition of $R_{uv,ref}$ in Eqs. (21) into (20), the dimensionless mean momentum equation becomes

$$0 = \frac{dV^*}{d\xi} - \left[2A_u\frac{V_{o'}}{V_{ref}}\right]\frac{dU^*}{d\xi} + 2A_u\left(U^*\frac{dV^*}{d\xi} - V^*\frac{dU^*}{d\xi}\right) + \frac{dR^*_{uv}}{d\xi}. \tag{22}$$

The nominal orders of magnitude of the terms on the right side of Eq. (22) are 1, B, $2A_u$, and 1, respectively. Hence, Eq. (22) satisfies the requirement of an admissible scaling. For the case of small normalized velocity difference $A_u \ll 1$ ($U_l \approx U_h$), the second and third terms on the right side of Eq. (22) become high order terms and do not contribute to the force balance.

Applying Eq. (17) for $dV^*/d\xi$, it can be shown that the first two terms in Eq. (22) sum up to

$$\frac{dV^*}{d\xi} - \left[2A_u\frac{V_{o'}}{V_{ref}}\right]\frac{dU^*}{d\xi} = \xi\frac{dU^*}{d\xi} + \left[B - 2A_u\frac{V_{o'}}{V_{ref}}\right]\frac{dU^*}{d\xi}. \tag{23}$$

While the term in the parenthesis in Eq. (22) can be rewritten as

$$U^*\frac{dV^*}{d\xi} - V^*\frac{dU^*}{d\xi} = B\frac{d(U^*)^2}{d\xi} + 2\xi U^*\frac{dU^*}{d\xi} - \frac{d(U^*V^*)}{d\xi}. \tag{24}$$

Hence, the admissible scaling for the mean momentum Eq. (22) can be written as

$$0 = \xi\frac{dU^*}{d\xi} + \left[B - 2A_u\frac{V_{o'}}{V_{ref}}\right]\frac{dU^*}{d\xi}$$
$$+ 2A_u\left(B\frac{d(U^*)^2}{d\xi} + 2\xi U^*\frac{dU^*}{d\xi} - \frac{d(U^*V^*)}{d\xi}\right) + \frac{dR^*_{uv}}{d\xi}. \tag{25}$$

An equation for the location of the maximum Reynolds shear stress can be obtained by setting $dR^*_{uv}/d\xi = 0$ in Eq. (25). In general, Eq. (25) indicates that the maximum Reynolds shear stress location does not coincide with o' or $\xi = 0$. By assuming that the peak Reynolds shear stress coincides with o', Pope obtained a simple expression for B [see Eqs. (5.217) and (5.222) of Ref. 2].

Integrating the mean momentum Eq. (25) from $\xi = -\infty$ to $\xi = \infty$ and applying boundary conditions yields

$$V^*_\infty + V^*_{-\infty} = \frac{1}{A_u}\int_{-\infty}^{\infty}\left(\xi\frac{dU^*}{d\xi}\right)d\xi + 4\int_{-\infty}^{\infty}\left(\xi U^*\frac{dU^*}{d\xi}\right)d\xi$$
$$+ \left(\frac{B}{A_u} - 2\frac{V_{o'}}{V_{ref}}\right). \tag{26}$$

Combining with Eq. (19), $V^*_{-\infty}$ can be obtained as

$$V^*_{-\infty} = -\frac{B}{2} + 2\int_{-\infty}^{\infty}\left(\xi U^*\frac{dU^*}{d\xi}\right)d\xi$$
$$+ \left(\frac{1}{2A_u} - \frac{1}{2}\right)\int_{-\infty}^{\infty}\left(\xi\frac{dU^*}{d\xi}\right)d\xi + \left(\frac{B}{2A_u} - \frac{V_{o'}}{V_{ref}}\right). \tag{27}$$

Hence, the analytical Eq. (18) for V^* can be presented as

$$V^* = BU^* + \int_{-\infty}^{\xi}\left(\xi\frac{dU^*}{d\xi}\right)d\xi + 2\int_{-\infty}^{\infty}\left(\xi U^*\frac{dU^*}{d\xi}\right)d\xi$$
$$+ \left(\frac{1}{2A_u} - \frac{1}{2}\right)\int_{-\infty}^{\infty}\left(\xi\frac{dU^*}{d\xi}\right)d\xi + \left(\frac{B}{2A_u} - \frac{V_{o'}}{V_{ref}}\right). \tag{28}$$

By definition, the normalized mean transverse velocity at $\xi = 0$ is zero: $V^*|_{\xi=0} = (V_{o'} - V_{o'})/V_{\rm ref} = 0$. Hence, Eq. (28) gives an equation for $V_{o'}/V_{\rm ref}$ as

$$\frac{V_{o'}}{V_{\rm ref}} = \int_{-\infty}^{0}\left(\xi\frac{dU^*}{d\xi}\right)d\xi + 2\int_{-\infty}^{\infty}\left(\xi U^*\frac{dU^*}{d\xi}\right)d\xi$$
$$+ \left(\frac{1}{2A_{\rm u}} - \frac{1}{2}\right)\int_{-\infty}^{\infty}\left(\xi\frac{dU^*}{d\xi}\right)d\xi + \frac{B}{2A_{\rm u}}. \quad (29)$$

Substituting $V_{o'}/V_{\rm ref}$ in Eqs. (29) into (28) produces an analytical equation for V^* as

$$V^* = BU^* + \int_{0}^{\xi}\left(\xi\frac{dU^*}{d\xi}\right)d\xi. \quad (30)$$

Solution for the scaled Reynolds shear stress can be obtained through integration of Eq. (25) and use of Eqs. (27) and (28) as

$$R_{uv}^* = -\int_{-\infty}^{\xi}\left(\xi\frac{dU^*}{d\xi}\right)d\xi + A_{\rm u}\left[2U^*\int_{-\infty}^{\xi}\left(\xi\frac{dU^*}{d\xi}\right)d\xi\right.$$
$$- 4\int_{-\infty}^{\xi}\left(\xi U^*\frac{dU^*}{d\xi}\right)d\xi + 2\int_{-\infty}^{\infty}\left(\xi U^*\frac{dU^*}{d\xi}\right)d\xi$$
$$+ 4U^*\int_{-\infty}^{\infty}\left(\xi U^*\frac{dU^*}{d\xi}\right)d\xi$$
$$\left. + \left(\frac{1}{A_{\rm u}} - 1\right)\left(U^* + \frac{1}{2}\right)\int_{-\infty}^{\infty}\left(\xi\frac{dU^*}{d\xi}\right)d\xi\right]. \quad (31)$$

Therefore, R_{uv}^* is a function of ξ and $A_{\rm u}$ only. In other words, the properly scaled Reynolds shear stress R_{uv}^* also approaches a self-similar state. However, the self-similar function of R_{uv}^* is not universal, but varies with $A_{\rm u}$.

III. COMPARISON WITH EXPERIMENTAL DATA

As the mixing layer growth rate $d\delta/dx$ and the growth ratio B play an important role in the scaling of the equations [see Eqs. (15) and (17)], we first examine the experimental data for $d\delta/dx$ and B. Next, approximate functions for V^* and R_{uv}^* are derived and compared with the experimental data.

A. Growth rate of mixing layer width

A number of definitions have been developed to measure mixing layer width, including visual thickness, thickness based on the distance between the locations where the mean velocity reaches a certain percentage of the average velocity, and thickness related to the vorticity of the flow. Benefits and shortcomings of the various measures of mixing layer thickness were discussed by Samimy and Elliott.[54] Examples of mixing layer width definition as summarized by Yoder[55] are listed in Table III. Not surprisingly, the variety of definition of mixing layer width has added to the complexity of comparing data from different experimental studies.

Building on a chain of physical arguments, Abramovich *et al.* (Ref. 38, pp. 36–42) derived a linear relation between the mixing layer growth rate and $A_{\rm u}$ as (see also Ref. 2, p. 142)

$$\frac{d\delta}{dx} = cA_{\rm u} \quad\text{or}\quad \frac{1}{A_{\rm u}}\frac{d\delta}{dx} = c, \quad (32)$$

TABLE III. Definitions of mixing layer width as summarized by Yoder (Ref. 55, pp. 11–14). Note that Yoder defined the dimensionless mean axial velocity as $(U - U_l)/(U_h - U_l)$, which varies between 0 and 1 and can be obtained by adding 0.5 to our definition of U^* in Eq. (7). The growth rate at $A_{\rm u} = 1$ is calculated using $\sigma_0 = 11$ (see Appendix A for the definition of σ_0).

Symbol	Definition	Ratio	$\left.\dfrac{d\delta}{dx}\right|_{A_{\rm u}=1}$
$\delta_{0.01}$	$y_{U^*=0.49} - y_{U^*=-0.49}$	$\dfrac{\delta_{0.01}}{(x - x_0)} = \dfrac{3.29}{\sigma}$	0.30
$b = \delta_{0.1}$	$y_{U^*=0.4} - y_{U^*=-0.4}$	$\dfrac{b}{(x - x_0)} = \dfrac{1.812}{\sigma}$	0.165
δ_{ω}	$\dfrac{U_h - U_l}{(\partial U/\partial y)_{\max}}$	$\dfrac{\delta_{\omega}}{(x - x_0)} = \dfrac{\sqrt{\pi}}{\sigma}$	0.161
δ_{u^2}	$y_{(U^*+0.5)^2=0.9} - y_{(U^*+0.5)^2=0.1}$	$\dfrac{\delta_{u^2}}{(x - x_0)} = \dfrac{1.488}{\sigma}$	0.135
$\delta_{\rm vis}$	Visual	$\dfrac{\delta_{\rm vis}}{(x - x_0)} = \dfrac{2\sqrt{\pi}}{\sigma}$	0.322

where c is a constant [note c is twice of the S in Eq. (5.209) of Ref. 2]. The same relation was proposed by Sabin.[39] The Abramovich–Sabin relation can also be derived directly from Görtler's similarity solution. Other relations have been proposed for the mixing layer growth rate, as listed in Table IV. After critically reviewing a number of data sets, Birch and Eggers[8] concluded that experimental data support the Abramovich–Sabin prediction expressed in Eq. (32).

In Birch and Eggers' Fig. 4 (see Ref. 8), the growth rate data are plotted as σ_0/σ vs $r = U_l/U_h$. The validity of Abramovich–Sabin prediction Eq. (32) was evaluated by plotting a $y = 1/x$ curve. Following the suggestion of Kline, Birch and Eggers replotted the growth rate data as σ_0/σ vs $A_{\rm u}$ (in their paper, the normalized velocity difference is denoted by the symbol λ). The validity of the Abramovich–Sabin prediction can then be evaluated by plotting a straight line through the origin.

In the new scale for the Reynolds shear stress [see Eq. (21)], the mixing layer growth rate is grouped with $A_{\rm u}$ as $\frac{1}{2A_{\rm u}}\frac{d\delta}{dx}$. In Fig. 3, the experimental $\frac{1}{2A_{\rm u}}\frac{d\delta}{dx}$ are plotted as a function of $A_{\rm u}$. The experimental data are compiled from those presented in the figures of Birch and Eggers[8] and Mehta.[16] If the Abramovich–Sabin prediction is valid, then $\frac{1}{2A_{\rm u}}\frac{d\delta}{dx}$ will be a constant, independent of $A_{\rm u}$. However, Fig. 3 shows that the Abramovich–Sabin prediction is valid only at $A_{\rm u} \gtrsim 0.2$, with $\frac{1}{2A_{\rm u}}\frac{d\delta}{dx} \approx 0.08$. As $A_{\rm u}$ approaches 0 (two streams with the same speed), $\frac{1}{2A_{\rm u}}\frac{d\delta}{dx}$ rises sharply. Mathematically, it is not clear if this rising

TABLE IV. Approximation function for the mixing layer growth rate. σ_0 is the spreading parameter at $A_{\rm u} = 1$. $r = U_l/U_h$ refers to the velocity ratio of the two streams. In the studies of Brown and Roshko,[9] densities of the two streams are different, and s is the density ratio. For two streams with the same density, $s = 1$.

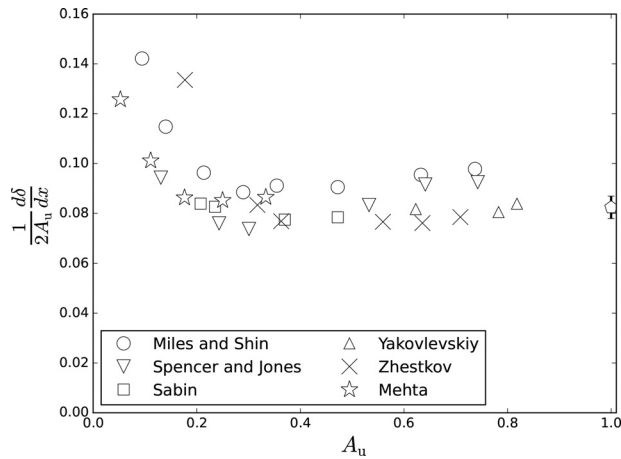| Miles and Shih[56]	Yule[33]	Brown and Roshko[9]
$\dfrac{d\delta}{dx} = \dfrac{1}{\sigma_0}\dfrac{1}{1 + 5r^2}$	$\dfrac{d\delta}{dx} = \dfrac{1}{\sigma_0}\dfrac{1 - r}{(1 + r)^{1/2}}$	$\dfrac{d\delta}{dx} = \dfrac{1}{\sigma_0}\dfrac{(1 - r)(1 + \sqrt{s})}{2(1 + r\sqrt{s})}$

FIG. 3. Growth rate of the width of planar turbulent mixing layers. Experimental data are compiled from figures in Birch and Eggers[8] and experiment of Mehta.[16] The error bar at $A_u = 1$ follows the values suggested by Birch and Eggers.[8]

FIG. 4. Experimental data of $B = (dy_{0.5}/dx)/(d\delta/dx)$. Values of B at $A_u = 0.37$ and $A_u = 1.0$ are calculated from table in Mehta and Westphal;[14] Values of B at $A_u = 0.41, 0.61, 0.67$ are calculated from data in experiments by Chang and coworkers.[25,26,57]

trend is bounded or not. Physically, as $A_u \to 0$, there will not be a mixing layer to be developed, i.e., $d\delta/dx \to 0$.

B. Ratio of growth rates $B = \frac{dy_{0.5}/dx}{d\delta/dx}$

In Sec. II A, we have shown that B, the ratio between the shifting speed of centerline and the growth rate of the mixing layer, plays an important role in the scaling of the mixing layer. That is, for V^* to be self-similar, B has to be a constant. Empirically, it has been observed that, in the mixing layer far downstream from its initiation, both the mixing layer width δ and the $y_{0.5}$ locations vary approximately linearly with x. Therefore, it is reasonable to assume that B is indeed close to a constant in the far field of a high Reynolds number turbulent mixing layer.

To obtain experimental data on B, evolution of both the mixing layer thickness $\delta(x)$ and the mixing layer centerline location $y_{0.5}(x)$ have to be measured. In nearly all mixing layer experiments, $\delta(x)$ is measured and reported. However, very few experiments report $y_{0.5}(x)$ data. Therefore, available B data are scarce, especially for the cases at low A_u. Figure 4 presents a few data points of B as a function of A_u.

When $A_u > 0.6$, B is approximately a constant of $B \approx -0.25$. As A_u decreases toward 0, B also approaches 0. There are not enough data points to establish the trend of B at small A_u. However, as A_u approaches zero ($U_l \approx U_h$), the mixing layer, if exists, will become more symmetric or $dy_{0.5}/dx \to 0$. Hence, B will approach zero for $A_u \to 0$.

Setting $dV^*/d\xi = 0$ in Eq. (17), the minimum V^* location can be found as

$$B = -\xi|_{V^*_{\min}}. \qquad (33)$$

Therefore, B is directly related to the location of the minimum V^*.

C. Mean axial flow data U^*

Experimental mean axial velocity data in planar turbulent mixing layers exhibit a sigmoid shape,[2] as shown in Fig. 5. Traditionally, the error function has been used to approximate U^*. Another choice is a hyperbolic tangent function $\tanh(\xi)$. For the convenience of obtaining
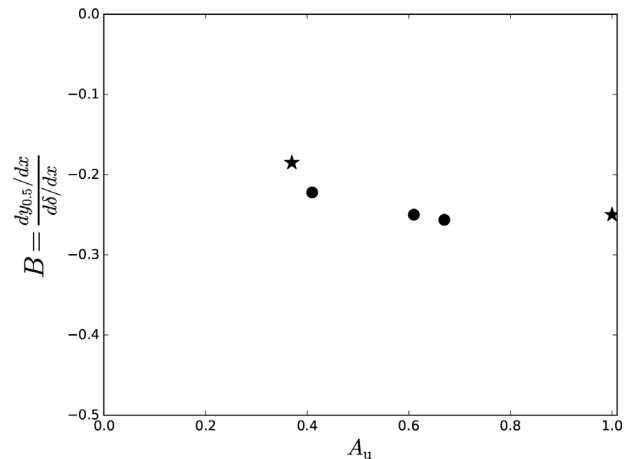
derivatives and integrals, here the error function is used to approximate U^* as

$$U^* \approx \frac{1}{2}\mathrm{erf}\left(\frac{\xi}{a}\right), \qquad (34)$$

where $a \approx 0.5518$ follows from the definition of $U^*(\xi = \pm 0.5) = \pm 0.4$.

Experimental U^* at three A_u are compared with the error function of Eq. (34) in Fig. 5. Overall, the error function fits the experimental data reasonably well. For the lowest $A_u = 0.053$, Mehta[16] observed that the splitter plate wake plays an important and lasting role in the development of the mixing layer. The small deviation from the error function at $A_u = 0.053$ may be due to the proximity to the end of the
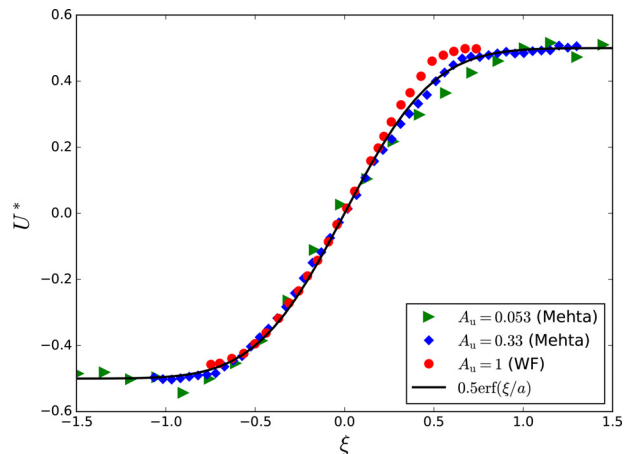

FIG. 5. Mean axial velocity distribution. The experimental data of $A_u = 0.053$ and 0.33 are from Mehta.[16] The streamwise location of the measurement is $x = 2.67$ m for the case of $A_u = 0.053$, and $x = 2.05$ m for the case of $A_u = 0.33$. The data of $A_u = 1$ are from Wygnanski and Fiedler[7] at the streamwise location of $x = 0.59$ m. The solid curve represents the approximating Eq. (34) using an error function.

splitter plate. Of the three A_u, experimental data at $A_u = 0.33$ agree best with the error function. At $A_u = 1$, the error function fits the experimental data well on the low speed side but underpredicts the data slightly on the high speed side.

It is logical to assume that as A_u approaches 0, the shape of the U^* profile would become anti-symmetric. At $A_u = 1$ the experimental U^* profile seems to deviate slightly from anti-symmetry. Nevertheless, the deviation from the error function is still relatively small even at $A_u = 1$ (see the WF data in Fig. 5).

D. Mean transverse flow data, V^*

Using an error function for U^*, an approximate function for the scaled mean transverse velocity can be obtained from Eq. (30) as (see Appendix B for details on the integrals),

$$V^*(\xi) \approx \frac{B}{2}\,\mathrm{erf}\left(\frac{\xi}{a}\right) - \frac{a}{2\sqrt{\pi}}e^{-\frac{\xi^2}{a^2}} + \frac{a}{2\sqrt{\pi}}. \tag{35}$$

In physical experiment or numerical simulations, the mean transverse velocity V is directly measured or computed, and the shifting speed of the centerline $V_{o'}$ is not known a priori. Therefore, it is more convenient to present the mean transverse flow data directly as V/V_{ref},

$$\frac{V}{V_{ref}} = V^* + \frac{V_{o'}}{V_{ref}} \approx \frac{B}{2}\,\mathrm{erf}\left(\frac{\xi}{a}\right) - \frac{a}{2\sqrt{\pi}}e^{-\frac{\xi^2}{a^2}} + \frac{a}{2\sqrt{\pi}} + \frac{B}{2A_u}. \tag{36}$$

In turbulent mixing layers, the mean transverse velocity is much smaller than the mean axial velocity, and its magnitude is often beyond the accuracy range of the currently available measuring techniques. Therefore, experimental V^* data are very scarce, and the uncertainty in the few available measurements is not clear. We first present the shapes of approximate Eq. (35) for V^* in Fig. 6(a) and the approximate Eq. (36) for V/V_{ref} in Fig. 6(b). As no data of B is available for $A_u < 0.3$ (see Fig. 4), the three A_u presented in Fig. 6 are $A_u = 1.0, 0.5$ and $A_u = 0.37$. The B values used in calculating the curves in Fig. 6 are $B = -0.25$ for $A_u = 1$, $B = -0.22$ for $A_u = 0.5$, and $B = -0.18$ for $A_u = 0.37$ (see Fig. 4).
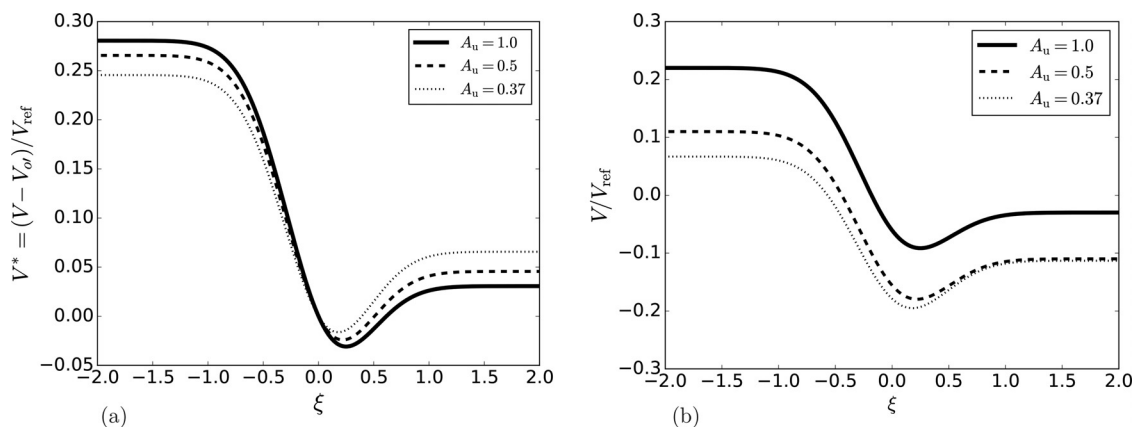
By comparing data from different experiments on turbulent mixing layers, one possible confusion is how the transversal direction is defined. For example, Wygnanski and Fielder[7] defined the positive y (or ξ) direction from the high speed side to the low speed side. Other experiments define the positive y (or ξ) direction from the low speed side to the high speed side. The latter is used in this work. In the transverse direction, fluid from the two sides is engulfed toward the middle of the mixing layer. Thus, in the present coordinate system, $V_\infty < 0$ and $V_{-\infty} > 0$.

In Fig. 7, experimental V/V_{ref} at two A_u are compared with Eq. (36). The difference between the experimental data and the approximate equation is not small. Given the large uncertainty in the measurement of V, this is not surprising. Nevertheless, Eq. (36) seems to capture well the shape of the mean transverse velocity. More experimental and numerical simulation data are required to evaluate the validity of Eq. (36).

E. Kinematic Reynolds shear stress data

Using an error function for U^*, an approximate function for R_{uv}^* can be obtained from Eq. (31) as (see Appendix B for details on the integrals),

$$R_{uv}^* \approx \frac{a}{2\sqrt{\pi}}\left\{ e^{-\xi^2/a^2} + A_u\left[\mathrm{erf}(\xi/a)e^{-\xi^2/a^2} \right.\right.$$
$$\left.\left. + \sqrt{2}\left(\mathrm{erf}(\xi/a) - \mathrm{erf}\left(\sqrt{2}\xi/a\right)\right)\right]\right\}. \tag{37}$$

Note that Eq. (37) does not involve the parameter B explicitly. In other words, the normalized Reynolds shear stress does not depend directly on B. It is not clear how the accuracy of the simplified Reynolds shear stress Eq. (37) is influenced approximating U^* with an error function. The validity of Eq. (37) is evaluated by experimental data. Shapes of the approximate Eq. (37) are presented in Fig. 8(a) for three values of A_u.

As A_u approaches 0, Eq. (37) indicates that the scaled Reynolds shear stress can be approximated by a Gaussian function as

FIG. 6. (a) Approximate Eq. (35) for $V^* = (V - V_{o'})/V_{ref}$ at three A_u. (b) Approximate Eq. (36) for V/V_{ref}. In the present coordinate system (y or ξ goes from the slow speed side to the high speed side), V_∞ is negative, as the high-speed fluid is moving downward toward the center of the mixing layer, and $V_{-\infty}$ is positive, as the slow-speed fluid is moving upward.
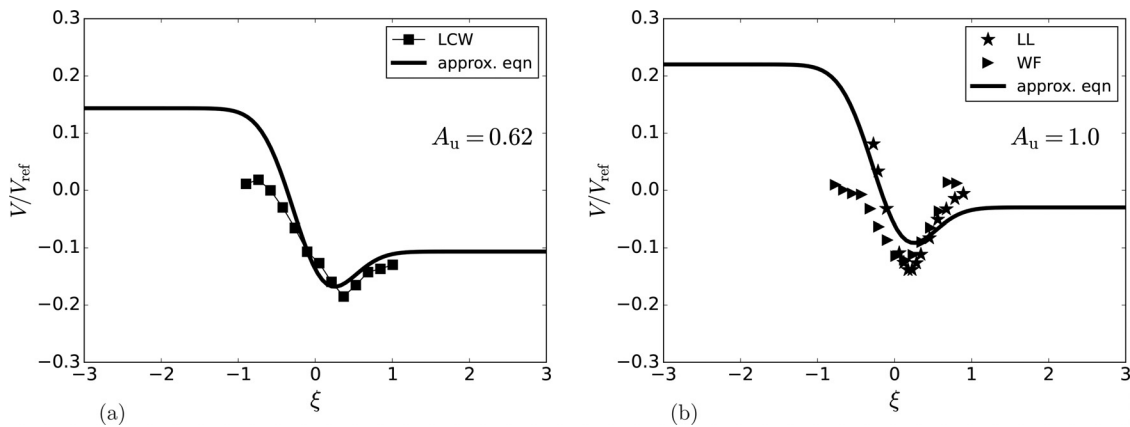
FIG. 7. Comparison of experimental V/V_{ref} with approximate Eq. (36) at two A_u values. (a) At $A_u = 0.62$ (LCW: experimental data by Li *et al.*[23] at the streamwise location of $x = 0.05$ m). (b). At $A_u = 1.0$ (LL: experimental data by Liepmann and Laufer[6] at the streamwise location of $x = 0.543$ m. WF: Wygnanski and Fielder[7] at the streamwise location of $x = 0.49$ m).

$$R_{uv}^* \approx \frac{a}{2\sqrt{\pi}} e^{-\xi^2/a^2}. \qquad (38)$$

Thus, the scaled Reynolds shear stress for $A_u = 0$ is symmetric around $\xi = 0$, as shown in Fig. 8(a) and the asymptotic peak value of R_{uv}^* is around 0.156 and occurs at $\xi = 0$.

As the normalized velocity difference A_u increases, the peak values of R_{uv}^* increase slightly and peak location shifts slightly toward the high speed side. At $A_u = 1$, the peak value of the Reynolds shear stress is $R_{uv}^*|_{max} \approx 0.163$ and the peak location is $\xi \approx 0.116$, as shown in Fig. 8(a).

Figure 8(b) shows the new scaling of the Reynolds shear stress data from the experimental measurement of Mehta.[14] Overall, the shapes of the scaled experimental data are similar to those in Fig. 8(a), but the difference and scatter are noticeable. For the case of $A_u = 0.33$, the difference between the scaled peak value and prediction is about 20%.

Given the critical role of Reynolds shear stress in the understanding and modeling of turbulent flows, we will examine next the

maximum value of Reynolds shear stress in the turbulent mixing layer and effects of the normalized velocity difference A_u.

1. Effects of A_u on the shapes of the kinematic Reynolds shear stress

The effects of velocity difference on mixing layer development have been systematically investigated by Mehta.[14] The mean axial velocity, kinematic Reynolds shear stress, and variances in the axial and wall-normal directions at $A_u = 0.053, 0.11, 0.18, 0.25, 0.33$ were measured in the experiments. In previous studies of mixing layers, including Mehta's, the kinematic Reynolds shear stress data are commonly reported as R_{uv}/U_{ref}^2. For the convenience of comparison, therefore, Eq. (37) is rewritten as

$$\frac{R_{uv}}{U_{ref}^2} \approx \left[\frac{d\delta}{dx}\frac{1}{2A_u}\right]\frac{a}{2\sqrt{\pi}}\left\{e^{-\xi^2/a^2} + A_u\left[\text{erf}(\xi/a)e^{-\xi^2/a^2}\right.\right.$$
$$\left.\left. + \sqrt{2}\left(\text{erf}(\xi/a) - \text{erf}\left(\sqrt{2}\xi/a\right)\right)\right]\right\}. \qquad (39)$$
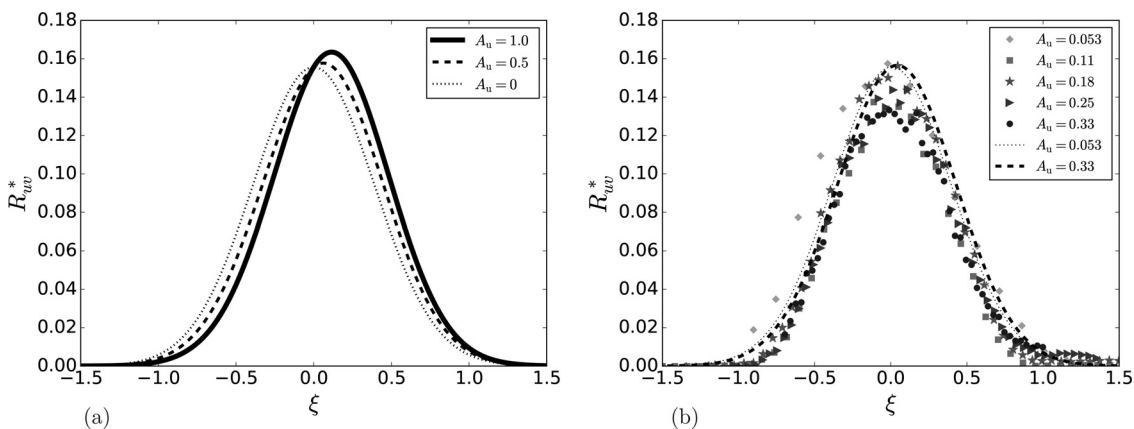

FIG. 8. (a) New scaled kinematic Reynolds shear stress $R_{uv}^* = R_{uv}/U_{avg}V_{ref}$ at three A_u using Eq. (37). (b) Experimental data of Reynolds shear stress normalized by the new scaling. The experimental data are from Mehta.[14] The streamwise location of the measurement is $x = 2.67$ m. The dotted curve at $A_u = 0.053$ and the dashed curve at $A_u = 0.33$ are from the approximating Eq. (37).
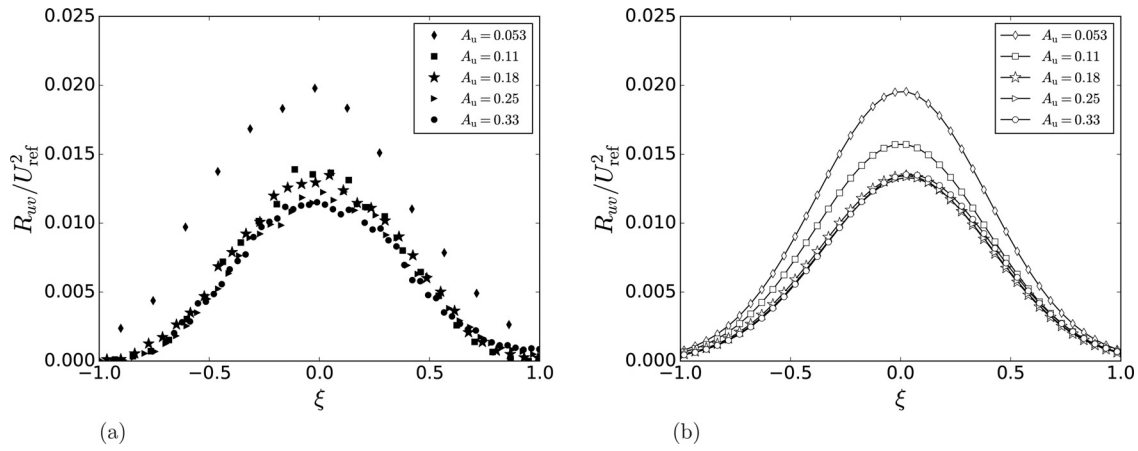
FIG. 9. (a) Reynolds shear stress profiles normalized by $(U_h - U_l)^2$ from experiments of Mehta.[16] The streamwise location of the measurement is $x = 2.67$ m. (b). Reynolds shear stress profiles calculated from the approximation Eq. (39), using $\frac{d\delta}{dx}\frac{1}{2A_u}$ as reported by Mehta.[16]

In Fig. 9(a), Mehta's experimental measurements of the Reynolds shear stress data normalized by u_{ref}^2 are presented vs ξ for five different A_u. In Fig. 9(b), the approximate Eq. (39) is plotted for the corresponding A_u. Figures 9(a) and 9(b) show that the approximate Eq. (39) and experimental data exhibit qualitatively the same dependence on A_u. The most prominent feature in Fig. 9 is the higher peak values of R_{uv}/U_{ref}^2 at lower A_u. As A_u increases, the peak R_{uv}/U_{ref}^2 value decreases in both the experimental data and Eq. (39). Moreover, at lowest $A_u = 0.053$, the experimental data and Eq. (39) are roughly symmetric about $\xi = 0$. With increasing A_u, the peak R_{uv}/U_{ref}^2 location shifts slightly toward the positive ξ direction (high speed side).

2. Effect of A_u on the maximum Reynolds shear stress

An important quantity to evaluate the validity of a new scaling or modeling for the Reynolds shear stress is the scaling of its peak value. From Eq. (39), the peak value of Reynolds shear stress can be estimated as

$$\frac{1}{\left[\frac{1}{2A_u}\frac{d\delta}{dx}\right]}\frac{R_{uv}}{U_{ref}^2}\bigg|_{max} \approx \frac{a}{2\sqrt{\pi}} \approx 0.156 \quad \text{or} \quad \frac{R_{uv}}{U_{ref}^2}\bigg|_{max} \approx 0.156\left[\frac{1}{2A_u}\frac{d\delta}{dx}\right].$$

(40)

Using a similarity analysis, Townsend[1] derived a scaling for the peak value of Reynolds shear stress as (see also Mehta[16]),

$$\frac{R_{uv}}{U_{ref}^2}\bigg|_{max} \approx 0.155\frac{1}{2A_u}\frac{d\delta}{dx}.$$

(41)

Thus, the present analysis produces the same scaling for the peak Reynolds shear stress value as Townsend.

In Fig. 10, Mehta's experimental peak Reynolds shear stress data, $|\langle uv\rangle|_{max}/U_{ref}^2$, are presented as a function of A_u. To better show the correlation between $|\langle uv\rangle|_{max}/U_{ref}^2$ and $\left[\frac{d\delta}{dx}\frac{1}{2A_u}\right]$, the experimental $0.14\left[\frac{d\delta}{dx}\frac{1}{2A_u}\right]$ data are also plotted in Fig. 10. Despite scatter among different experimental studies, Fig. 10 displays an excellent correlation between $|\langle uv\rangle|_{max}/U_{ref}^2$ and $\left[\frac{d\delta}{dx}\frac{1}{2A_u}\right]$, indicating that $|\langle uv\rangle|_{max}/U_{ref}^2$

scales as $\left[\frac{d\delta}{dx}\frac{1}{2A_u}\right]$. However, the numerical factor 0.14 is about 10% lower than the prediction in Eqs. (40) or (41). The cause of the discrepancy is unclear; possible reasons include the use of an error function in the approximation function and/or in the definition and measurement of $d\delta/dx$ data.

IV. CONCLUSION

In this work, planar turbulent mixing layers are investigated by a scaling patch approach, and the main results are summarized in Table V. The effect of the velocity difference on the development of mixing layers is found to be best captured by the normalized velocity difference A_u. A prominent feature of a planar turbulent mixing layer is that the mean average location $y_{0.5}$ shifts toward the low speed stream side. The ratio B between the growth rate of the mixing layer $d\delta/dx$ and the shift rate of $dy_{0.5}/dx$ is found to an important parameter in the admissible scaling of the mean continuity equation.
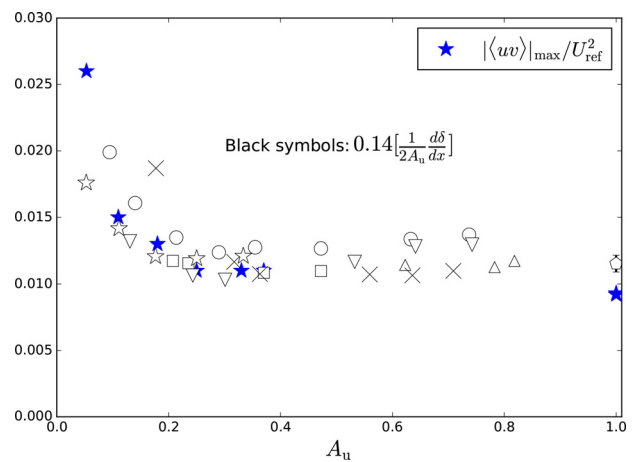

FIG. 10. Maximum values of Reynolds shear stress scaled by $(U_h - U_l)^2$. Black open symbols are $0.14\left[\frac{1}{2A_u}\frac{d\delta}{dx}\right]$. The experimental data are from Mehta.[16]

TABLE V. Summary of planar mixing layer results.

Normalized velocity difference	$A_{\mathrm{u}} = \dfrac{U_h - U_l}{U_h + U_l}$
Normalized transverse location	$\xi = \dfrac{y - y_{0.5}}{\delta}$
Characteristic scales	$U_{\mathrm{ref}} = U_h - U_l; \quad V_{\mathrm{ref}} = U_{\mathrm{ref}}\dfrac{d\delta}{dx}; \quad R_{uv,\mathrm{ref}} = U_{\mathrm{avg}}\,V_{\mathrm{ref}}$
Admissible scaling of continuity equation	$0 = -B\dfrac{dU^*}{d\xi} - \xi\dfrac{dU^*}{d\xi} + \dfrac{dV^*}{d\xi}, \quad \text{where } B = \dfrac{dy_{0.5}/dx}{d\delta/dx}$
Admissible scaling of momentum equation	$0 = \dfrac{dV^*}{d\xi} - 2A_u\dfrac{V_{o'}}{V_{\mathrm{ref}}}\dfrac{dU^*}{d\xi} + 2A_{\mathrm{u}}\left(U^*\dfrac{dV^*}{d\xi} - V^*\dfrac{dU^*}{d\xi}\right) + \dfrac{dR_{uv}^*}{d\xi}.$
Approximate equation for V^*	$V^* \approx \dfrac{B}{2}\,\mathrm{erf}\left(\dfrac{\xi}{a}\right) - \dfrac{a}{2\sqrt{\pi}}e^{-\frac{\xi^2}{a^2}} + \dfrac{a}{2\sqrt{\pi}}, \quad \text{where } a = 0.5518$
Approximate equation for R_{uv}^*	$R_{uv}^* \approx \dfrac{a}{2\sqrt{\pi}}\left\{e^{-\xi^2/a^2} + A_{\mathrm{u}}\left[\mathrm{erf}(\xi/a)e^{-\xi^2/a^2} + \sqrt{2}\left(\mathrm{erf}(\xi/a) - \mathrm{erf}\left(\sqrt{2}\xi/a\right)\right)\right]\right\}.$

In previous studies of turbulent free-shear flow, the properties of the mean transverse flow rarely received attention, and the mean continuity equation is typically integrated to remove the mean transverse flow from the analysis. A proper scale for the mean transverse flow is identified here as $V_{\mathrm{ref}} = (U_h - U_l)d\delta/dx$. Moreover, we show that the proper scale for the Reynolds shear stress is a mixed scale of the average axial U_{avg} and the transverse velocity scale V_{ref}. Hence, the proper scale for the Reynolds shear stress is directly related to the velocity scale for the mean transverse flow.

Approximate equations have been developed for the mean transverse flow and Reynolds shear stress. At the limit of $A_{\mathrm{u}} \to 0$, the Reynolds shear stress profile can be approximated by a simple Gaussian function. At larger A_{u}, the shape of the Reynolds shear stress profile is close to a Gaussian function, but its maximum location does not coincide with the location of the mean axial velocity. The effect of A_{u} on the magnitude and shape of the mean transverse flow and Reynolds shear stress have been examined.

The present analysis demonstrates that the scaling patch approach, originally developed for wall-bounded turbulence, can also be applied to free-shear turbulence, including planar turbulent mixing layers. One challenge in current studies of turbulent flow is the prediction of turbulent boundary layers under adverse pressure gradient (APG TBL). Given that the mean streamwise velocity and Reynolds shear stress distributions in planar turbulent mixing layers and the outer region of APG TBL present close similarities, the present analysis of mixing layers could be considered for application to APG TBL.

AUTHOR DECLARATIONS
Conflict of Interest

The authors have no conflicts to disclose.

Author Contributions

Tie Wei: Conceptualization (equal); Data curation (equal); Formal analysis (equal); Writing – original draft (equal); Writing – review & editing (equal). **Zhaorui Li:** Conceptualization (equal); Data curation (equal); Formal analysis (equal); Writing – original draft (equal); Writing – review & editing (equal). **Daniel Livescu:** Conceptualization (equal); Data curation (equal); Formal analysis (equal); Writing – original draft (equal); Writing – review & editing (equal).

APPENDIX A: DEFINITION OF MIXING LAYER GROWTH RATE

The mixing layer growth rate is defined here as $d\delta/dx$, where δ is the mixing layer width. In order to fit an error function to the U^* data, another parameter a is used in Eq. (34). Thus the self-similar parameter used in this work is

$$\frac{\xi}{a} = \frac{y}{\delta a}. \tag{A1}$$

In most previous studies of turbulent mixing layer flows (e.g., Birch and Eggers[8] and Mehta[16]), the self-similar variable is defined as

$$\zeta \overset{\text{def}}{=} \sigma\frac{y}{x}, \tag{A2}$$

where σ is called the spreading parameter.

Comparing Eqs. (A1) and (A2), the spreading parameter used in the previous studies is related to the mixing layer growth rate as

$$\frac{1}{\sigma} = a\frac{d\delta}{dx} \quad \text{or} \quad \frac{1}{\sigma} = \frac{1}{a\dfrac{d\delta}{dx}}. \tag{A3}$$

At $A_{\mathrm{u}} = 1$, the spreading parameter is

$$\frac{1}{\sigma_0} = a\frac{d\delta}{dx}\bigg|_{A_{\mathrm{u}}=1}. \tag{A4}$$

The ratio σ_0/σ used in Birch and Eggers's paper is

$$\frac{\sigma_0}{\sigma} = \left[\frac{1}{\left. \dfrac{d\delta}{dx} \right|_{A_u=1}} \right] \frac{d\delta}{dx}. \tag{A5}$$

Birch and Eggers[8] suggested an optimum value of $\sigma_0 = 11$. However, they also pointed out that the optimum value of σ_0 may be less than 11 in turbulent mixing layers with tripped initial boundary layers. In contrast, Mehta and Westphal[14] reported a larger growth rate in a mixing layer without a trip wire. The difference in the σ_0 or $d\delta/dx$ from the presence of trip wire may cause discrepancy in the prediction of the peak Reynolds shear stress value.

APPENDIX B: INTEGRALS INVOLVING THE ERROR FUNCTION

In Sec. III C, the error function is used to approximate the mean axial velocity in planar turbulent mixing layers $U^* = 0.5\mathrm{erf}(\xi/a)$. Then, the derivative of the mean axial velocity is

$$\frac{dU^*}{d\xi} = \frac{1}{a\sqrt{\pi}} e^{(-\xi^2/a^2)}. \tag{B1}$$

The following integrals are used in the derivation of the approximation functions for V^* and R_{uv}^* in Secs. III D and III E.

$$\int_{-\infty}^{\xi} \left(\xi \frac{dU^*}{d\xi} \right) d\xi = -\frac{a}{2\sqrt{\pi}} e^{(-\xi^2/a^2)}, \tag{B2a}$$

$$\int_{0}^{\xi} \left(\xi \frac{dU^*}{d\xi} \right) d\xi = -\frac{a}{2\sqrt{\pi}} e^{(-\xi^2/a^2)} + \frac{a}{2\sqrt{\pi}}, \tag{B2b}$$

$$\int_{-\infty}^{\infty} \left(\xi \frac{dU^*}{d\xi} \right) d\xi = 0, \tag{B2c}$$

$$\int_{-\infty}^{\xi} \left(\xi U^* \frac{dU^*}{d\xi} \right) d\xi = \frac{a}{8\sqrt{\pi}} \left(\sqrt{2}\mathrm{erf}\left(\sqrt{2}\xi/a\right) \right.$$
$$\left. - 2\mathrm{erf}(\xi/a) e^{(-\xi^2/a^2)} \right) + \frac{\sqrt{2}a}{8\sqrt{\pi}}, \tag{B2d}$$

$$\int_{-\infty}^{\infty} \left(\xi U^* \frac{dU^*}{d\xi} \right) d\xi = \frac{\sqrt{2}a}{4\sqrt{\pi}}. \tag{B2e}$$

REFERENCES

[1]A. A. Townsend, *The Structure of Turbulent Shear Flow* (Cambridge University Press, 1980).

[2]S. B. Pope, *Turbulent Flows* (Cambridge University Press, 2000).

[3]M. Van Dyke, *An Album of Fluid Motion* (Parabolic Press, Stanford, 1982).

[4]H. von Görtler, "Berechnung von aufgaben der freien turbulenz auf grund eines neuen näherungsansatzes," J. Appl. Math. Mech. **22**(5), 244–254 (1942).

[5]H. Schlichting and K. Gersten, *Boundary-Layer Theory* (Springer Science & Business Media, 2000).

[6]H. W. Liepmann and J. Laufer, "Investigations of free turbulent mixing," NACA Technical Report No. 1257, 1947.

[7]I. Wygnanski and H. E. Fiedler, "The two-dimensional mixing region," J. Fluid Mech. **41**(2), 327–361 (1970).

[8]S. F. Birch and J. M. Eggers, "A critical review of the experimental data for developed free turbulent shear layers," Report No. NASA SP-321, 1973.

[9]G. L. Brown and A. Roshko, "On density effects and large structure in turbulent mixing layers," J. Fluid Mech. **64**(4), 775–816 (1974).

[10]F. H. Champagne, Y. H. Pao, and I. J. Wygnanski, "On the two-dimensional mixing region," J. Fluid Mech. **74**(2), 209–250 (1976).

[11]I. Wygnanski, D. Oster, H. Fiedler, and B. Dziomba, "On the perseverance of a quasi-two-dimensional eddy-structure in a turbulent mixing layer," J. Fluid Mech. **93**(2), 325–335 (1979).

[12]J. J. Riley and R. W. Metcalfe, "Direct numerical simulation of a perturbed, turbulent mixing layer," AIAA Paper No. 1980-274, 1980.

[13]D. Oster and I. Wygnanski, "The forced mixing layer between parallel streams," J. Fluid Mech. **123**, 91–130 (1982).

[14]R. D. Mehta and R. V. Westphal, "An experimental study of plane mixing layer development," Report No. NASA-TM-86698, 1985.

[15]F. K. Browand and T. R. Troutt, "The turbulent mixing layer: Geometry of large vortices," J. Fluid Mech. **158**, 489–509 (1985).

[16]R. D. Mehta, "Effect of velocity ratio on plane mixing layer development: Influence of the splitter plate wake," Exp. Fluids **10**(4), 194–204 (1991).

[17]M. M. Rogers and R. D. Moser, "Direct simulation of a self-similar turbulent mixing layer," Phys. Fluids **6**(2), 903–923 (1994).

[18]B. Vreman, B. Geurts, and H. Kuerten, "Large-eddy simulation of the turbulent mixing layer," J. Fluid Mech. **339**, 357–390 (1997).

[19]I. C. C. Bruin, "Direct and large eddy simulation of the spatial turbulent mixing layer," Ph.D. thesis (University of Twente, 2001).

[20]B. J. Geurts and D. D. Holm, "Alpha-modeling strategy for LES of turbulent mixing," Fluid Mech. Appl. **66**, 237–272 (2002).

[21]M. A. Azim and A. S. Islam, "Plane mixing layers from parallel and non-parallel merging of two streams," Exp. Fluids **34**(2), 220–226 (2003).

[22]N. D. Sandham and R. D. Sandberg, "Direct numerical simulation of the early development of a turbulent mixing layer downstream of a splitter plate," J. Turbul. **10**, N1 (2009).

[23]C.-T. Li, K.-C. Chang, and M.-R. Wang, "PIV measurements of turbulent flow in planar mixing layer," Exp. Therm. Fluid Sci. **33**(3), 527–537 (2009).

[24]S. Laizet, S. Lardeau, and E. Lamballais, "Direct numerical simulation of a mixing layer downstream a thick splitter plate," Phys. Fluids **22**(1), 015104 (2010).

[25]K.-C. Chang and C.-T. Li, "Redefining mixing length in turbulent mixing layer in terms of shear-induced vorticity," J. Fluid Sci. Technol. **6**(4), 662–673 (2011).

[26]K.-C. Chang, K.-H. Li, and T.-C. Chang, "Re-evaluating mixing length in turbulent mixing layer by means of high-order statistics of velocity field," Int. J. Mod. Phys.: Conf. Ser. **19**, 154–165 (2012).

[27]A. Attili and F. Bisetti, "Statistics and scaling of turbulence in a spatially developing mixing layer at Reλ = 250," Phys. Fluids **24**(3), 035109 (2012).

[28]C. S. Martha, G. A. Blaisdell, and A. S. Lyrintzis, "Large eddy simulations of 2D and 3D spatially developing mixing layers," Aerosp. Sci. Technol. **31**(1), 59–72 (2013).

[29]O. R. H. Buxton and B. Ganapathisubramani, "Concurrent scale interactions in the far-field of a turbulent mixing layer," Phys. Fluids **26**(12), 125106 (2014).

[30]D. A. Yoder, J. R. DeBonis, and N. J. Georgiadis, "Modeling of turbulent free shear flows," Comput. Fluids **117**, 212–232 (2015).

[31]S. Suryanarayanan and R. Narasimha, "Insights into the growth rate of spatially evolving plane turbulent free-shear layers from 2D vortex-gas simulations," Phys. Fluids **29**(2), 020708 (2017).

[32]B. W. Spencer, "Statistical investigation of turbulent velocity and pressure fields in a two-stream mixing layer," Ph.D. thesis (University of Illinois at Urbana-Champaign, 1970).

[33]A. J. Yule, *Two-Dimensional Self-Preserving Turbulent Mixing Layers at Different Free Stream Velocity Ratios* (HM Stationery Office, 1972).

[34]J. Bell and R. Mehta, "Development of a two-stream mixing layer from tripped and untripped boundary layers," AIAA J. **28**(12), 2034–2042 (1990).

[35]J. Glimm, J. W. Grove, X. L. Li, W. Oh, and D. H. Sharp, "A critical analysis of Rayleigh–Taylor growth rates," J. Comput. Phys **169**(2), 652–677 (2001).

[36]D. Livescu, J. R. Ristorcelli, R. A. Gore, S. H. Dean, W. H. Cabot, and A. W. Cook, "High-Reynolds number Rayleigh–Taylor turbulence," J. Turbul. **10**, N13 (2009).

[37]T. Wei and D. Livescu, "Late-time quadratic growth in single-mode Rayleigh–Taylor instability," Phys. Rev. E **86**(4), 046405 (2012).

[38]G. N. Abramovich, T. A. Girshovich, S. Iu Krasheninnikov, A. N. Sekundov, and I. P. Smirnova, *The Theory of Turbulent Jets* (Izdatel Nauka, Moscow, 1963).

[39]C. M. Sabin, "An analytical and experimental study of the plane, incompressible, turbulent free-shear layer with arbitrary velocity ratio and pressure gradient," J. Basic Eng. **87**(2), 421–428 (1965).

[40]C. Pantano and S. Sarkar, "A study of compressibility effects in the high-speed turbulent shear layer using direct simulation," J. Fluid Mech. **451**, 329–371 (2002).

[41]T. Wei, P. Fife, J. Klewicki, and P. McMurtry, "Properties of the mean momentum balance in turbulent boundary layer, pipe and channel flows," J. Fluid Mech. **522**, 303–327 (2005).

[42]P. Fife, J. Klewicki, P. McMurtry, and T. Wei, "Multiscaling in the presence of indeterminacy: Wall-induced turbulence," Multiscale Model. Simul. **4**(3), 936–959 (2005).

[43]P. Fife, *Scaling Approaches to Steady Wall-Induced Turbulence* (2006).

[44]T. Wei, P. Fife, J. Klewicki, and P. McMurtry, "Scaling heat transfer in fully developed turbulent channel flow," Int. J. Heat Mass Transfer **48**(25–26), 5284–5296 (2005).

[45]A. Zhou, S. Pirozzoli, and J. Klewicki, "Mean equation based scaling analysis of fully-developed turbulent channel flow with uniform heat generation," Int. J. Heat Mass Transfer **115**, 50–61 (2017).

[46]F. Mehdi, J. C. Klewicki, and C. M. White, "Mean force structure and its scaling in rough-wall turbulent boundary layers," J. Fluid Mech. **731**, 682–712 (2013).

[47]T. Wei, "Properties of the mean momentum balance in turbulent Taylor–Couette flow," J. Fluid Mech. **891**, A10 (2020).

[48]T. Wei, "Multiscaling analysis of buoyancy-driven turbulence in a differentially heated vertical channel," Phys. Rev. Fluids **4**(7), 073502 (2019).

[49]T. Wei, "Analyses of buoyancy-driven convection," Adv. Heat Transfer **52**, 1–93 (2020).

[50]T. Wei and D. Livescu, "Scaling of the mean transverse flow and Reynolds shear stress in turbulent plane jet," Phys. Fluids **33**(3), 035142 (2021).

[51]T. Wei and D. Livescu, "Scaling patch analysis of turbulent planar plume," Phys. Fluids **33**(5), 055101 (2021).

[52]T. Wei, D. Livescu, and X. Liu, "Scaling patch analysis of planar turbulent wake," Phys. Fluids **34**, 065116 (2022).

[53]J. R. Baltzer and D. Livescu, "Variable-density effects in incompressible non-buoyant shear-driven turbulent mixing layers," J. Fluid Mech. **900**, A16 (2020).

[54]M. Samimy and G. S. Elliott, "Effects of compressibility on the characteristics of free shear layers," AIAA J. **28**(3), 439–445 (1990).

[55]D. Yoder, "Algebraic Reynolds stress modeling of planar mixing layer flows," Ph.D. thesis (University of Cincinnati, 2005).

[56]J. B. Miles and J.-S. Shih, "Similarity parameter for two-stream turbulent jet-mixing region," AIAA J. **6**, 1429 (1968).

[57]K.-C. Chang and K.-H. Lee, "Determination of mixing length in turbulent mixing layer on basis of vorticity field," Int. J. Heat Fluid Flow **66**, 121–126 (2017).